Barrier Winds Along the Sierra Nevada Mountains

THOMAS R. PARISH

Department of Atmospheric Science, University of Wyoming, Laramie 82071

(Manuscript received 5 November 1981, in final form 17 February 1982)

ABSTRACT

Observational evidence from instrumented aircraft, Doppler radar and rawinsondes suggest low-level, mountain-parallel jets are a common wintertime feature along the western slope of the Sierra Nevada Range and extending into the California Valley. It is proposed that the formation and maintenance of the low-level jet is a result of the pressure field created by the damming of stable air as it is forced up against the steep mountain barrier. Numerical experiments, using a two-dimensional (x, z) primitive equation model incorporating terrain representative of the Sierra Nevada Mountains, are carried out to test this assertion.

1. Introduction

The main objective of the Sierra Cooperative Pilot Project (SCPP) is to assess the potential of weather modification technology as a means of increasing the precipitation in the American River Basin region of the Sierra Nevada Mountains. In conjunction with SCPP, the University of Wyoming King Air (K/A) instrumented research aircraft has operated along the Sierra Nevada Range during the winter months of three previous field seasons, 1977–78, 1978–79 and 1979–80, in order to obtain an understanding of the microphysical and dynamical processes associated with wintertime storms. In pursuit of this goal, a large body of data has been gathered by the K/A during the numerous survey flights which have been conducted over the American River Basin area. Aside from a full complement of cloud physics probes, the K/A is also equipped with a Doppler navigation system, capable of determining the horizontal wind components with an accuracy of ± 1 m s^{-1}.

Among the significant results of the 1977–78 field season was the documentation of the low-level, mountain-parallel jet stream as a dominant phenomenon along the Sierra Nevada western slopes, extending into the California Valley. It was noted that a jet stream of 15 to 30 m s^{-1} develops below crest level ($\sim$2700 m) when a cold front and/or upper level trough approaches the mountains from the west. Moderate to severe turbulence was created from mechanical processes associated with the wind shear from the low-level jet (Marwitz *et al.*, 1978).

2. Observations of the low-level mountain-parallel jet

Fig. 1 is a composite of various hodographs obtained from the K/A during takeoff from McClellan Air Firce Base, located at the foot of the Sierra Nevada sloping terrain (see Fig. 2). In all cases, the strongest winds were found below 2000 m and were from the SSE, roughly parallel to the mountains. Further information can be obtained from rawinsonde stations near the target area. Rawinsonde ascents are made at Oakland, CA, Santa Clara, CA, Sheridan, CA, Fresh Pond, CA, Reno, NV and Winnemucca, NV, with only Oakland and Winnemucca being part of the National Weather Service operated network. Fig. 3 shows analyses of the mountain-parallel wind components for selected cases during February of 1979. Flight tracks from the K/A during the corresponding time periods have been plotted on each figure as well. The wind data collected from the K/A has been synthesized with the rawinsonde data to provide detailed resolution in the vicinity of the windward side of the mountains. In both cases the low level, mountain-parallel jet is apparent. The strongest winds are found $\sim$600–1500 m above ground level, quite representative of most cases in which the low level jets are found. The horizontal extent of the low-level jet is at least 100 km, reaching down from the Sierra Barrier into the California Valley. Magnitudes of the jet typically exceed 20 m s^{-1}. The corresponding wind components normal to the barrier are shown in Fig. 4. As the stable air is forced up the side of the Sierra Nevada Range, significant deceleration occurs. Near-stagnant normal components are commonly found in the lowest levels along the western side of the mountain. Occasionally a slight component directed away from the mountain can be observed, in striking contrast with the pattern of the synoptic pressure gradient.

3. Theoretical considerations

Low-level, mountain-parallel jet streams similar to those observed along the Sierra Nevada Range

0021-8952/82/070925-06$05.50

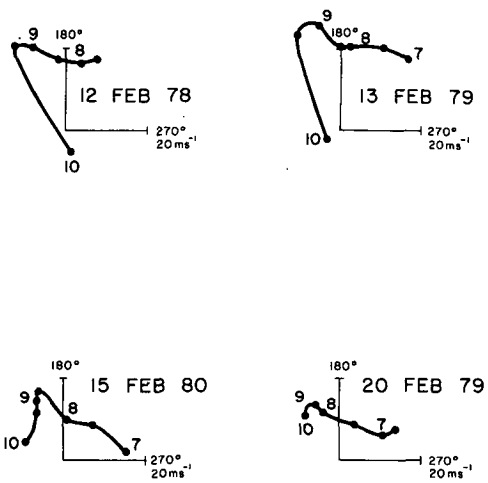

FIG. 1. Hodographs constructed from data collected by the K/A research aircraft during the SCPP program. Data are plotted at 5 kPa intervals starting at 100 kPa; the numbers refer to the level, 10 for 100 kPa, 9 for 90 kPa, etc.

are not particularly uncommon. Such features are frequently observed along the Brooks Range in Alaska (Schwerdtfeger, 1974) and in Antarctica, along the Antarctic Peninsula (Schwerdtfeger, 1975) and over the western Ross Ice Shelf near the Transantarctic Mountains. The Schwerdtfeger papers represent the original work on the topic. It has been known for many years that very persistent, strong mountain-parallel winds have haunted stations situated along the eastern side of the Antarctic Peninsula. The historic 1902–03 Swedish South Polar Expedition of Nordenskjöld (Nordenskjöld, 1911), which wintered two years along the Peninsula, encountered the same strong, low-level winds along nearly a 200 km stretch from 64 to 66°S. Until recently, such winds have been interpreted in terms of the large-scale pressure field. The Schwerdtfeger papers firmly established such conditions to be of a mesoscale, dependent on the stability of the atmosphere and steepness of adjacent mountain terrain. The explanation is as follows: whenever a large-scale component of wind is directed towards a mountain chain, the air is forced to rise over the barrier. Owing to the stability of the air, the forced ascent is resisted and appreciable deceleration occurs. This leads to a damming up of the stable air against the mountain and consequently an increase in pressure along the windward slopes. Schwerdtfeger (1979) estimates this daming effect may lead to a 400–800 Pa (4–8 mb) pressure increase in the Antarctic Peninsula region depending on the initial wind and temperature structure in the boundary layer away from the barrier. Such an orographic surplus of pressure along the windward mountain face has been discussed in Godske *et al.* (1957); numerical and analytic models reveal such a pressure anomaly (for example, Smith, 1979). The resulting damming leads to a pressure gradient force strikingly dissimilar to the large-scale conditions, being directed away from the mountains. If such conditions persist for periods of time exceeding a few hours, Coriolis effects become important. The local pressure field will then support geostrophic-type motion directed parallel to the mountains. Of course, friction and diabatic effects must also be considered, but their combined effect is probably only of secondary importance in modifying the barrier wind. Since the terrain acts to force such motion, the "barrier" winds are confined mainly to the levels below the crest and extend some distance away from the mountain, dependent on the pressure field provided by the mountain-damming. Schwerdtfeger (1979) estimates a width of at least 100 km for the Antarctic Peninsula barrier winds.

4. Numerical simulation of barrier winds

a. The model

In order to simulate barrier winds, an explicit hydrostatic two-dimensional (x, z) primitive equation model in terrain-following coordinates has been developed. Following Anthes and Warner (1978), the flux form of the horizontal equations of motion used in the model may be written

$$\frac{\partial p^* u}{\partial t} = -\frac{\partial p^* uu}{\partial x} - \frac{\partial p^* u\dot{\sigma}}{\partial \sigma} - p^*\left[\frac{RT}{(p^* + p_t/\sigma)}\frac{\partial p^*}{\partial x} + \frac{\partial \phi}{\partial x}\right] + p^* vf + FU, \quad (1)$$

$$\frac{\partial p^* v}{\partial t} = -\frac{\partial p^* uv}{\partial x} - \frac{\partial p^* v\dot{\sigma}}{\partial \sigma} - p^* f(u - u_g) + FV. \quad (2)$$

The vertical coordinate σ is given by

$$\sigma \equiv \frac{p - p_t}{p_s - p_t} \equiv \frac{p - p_t}{p^*}$$

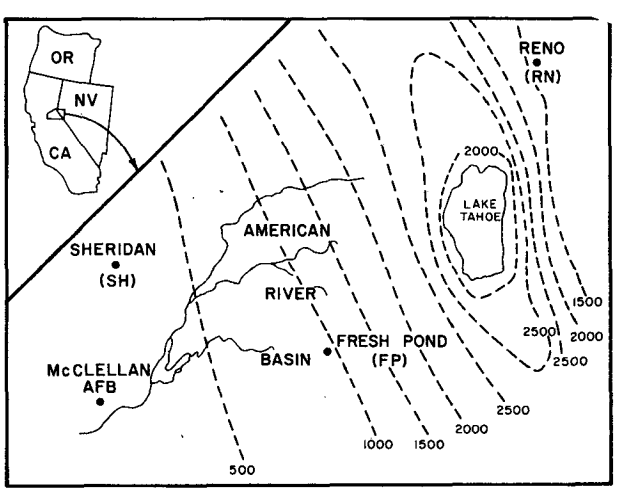

FIG. 2. Topography of the American River Basin, target area for SCPP. Contour heights in m.

and the "vertical" velocity term $\dot{\sigma}$ is simply given by

$$\dot{\sigma} = \frac{d\sigma}{dt}.$$

In the above equations p_t is the pressure at the top of the model (set at 25 kPa) and p_s is the surface pressure. The *FU* and *FV* terms refer to the time rate of change of the motion components due to sub-grid scale horizontal and vertical diffusion processes. All other symbols have their usual meteorological meaning. An advective form of the thermodynamic equation was used since it was found to be more stable than the flux form (Seaman and Anthes, 1981). Omitting the diabatic terms, it may be written

$$\frac{\partial T}{\partial t} = \frac{RT}{(p^*\sigma + p_t)}\frac{\sigma}{c_p}\frac{\partial p^*}{\partial t} - \dot{\sigma}\frac{\partial T}{\partial \sigma} + \frac{RTp^*}{(p^*\sigma + p_t)c_p}\dot{\sigma} - u\frac{\partial T}{\partial x} + \frac{RT\sigma}{(p^*\sigma + p_t)c_p}\frac{u}{}\frac{\partial p^*}{\partial x} + FT, \quad (3)$$

where FT refers to the time rate of change of temperature from sub-grid scale horizontal and vertical diffusion. The flux form of the continuity equation is

$$\frac{\partial p^*}{\partial t} = -\frac{\partial p^* u}{\partial x} - \frac{\partial p^* \dot{\sigma}}{\partial \sigma}. \quad (4)$$

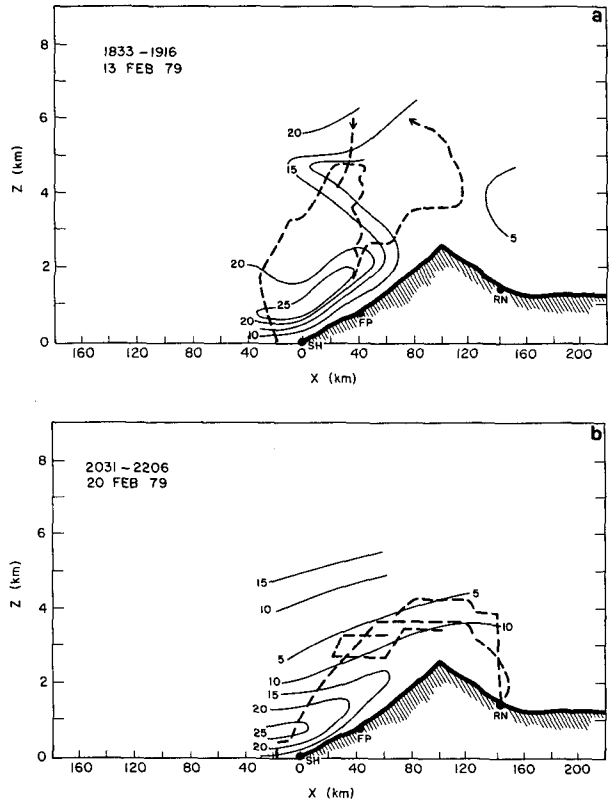

FIG. 3. Mountain-parallel motion components (m s^{-1}) derived from rawinsonde and K/A data for 13 and 21 February 1979. Flight track shown by dashed line; flight time listed at top.

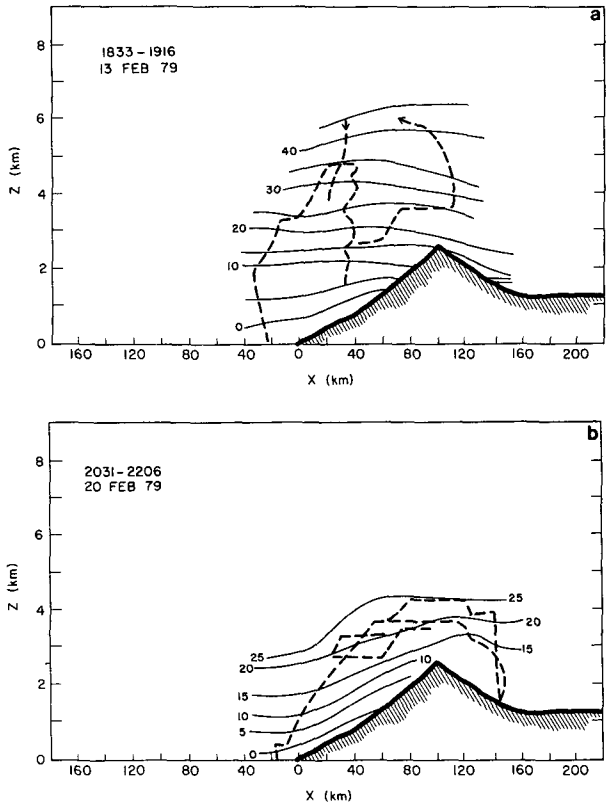

FIG. 4. As in Fig. 3, but for motion components (m s^{-1}) normal to the Sierra Nevada barrier.

The final equation needed to close the system is the hydrostatic equation

$$\frac{\partial \phi}{\partial \ln(\sigma + p_t/p^*)} = -RT. \quad (5)$$

The model equations are integrated using the centered in time (leapfrog) method. Horizontal diffusion of wind and temperature is modeled following Anthes and Warner (1978). The model employs a multilevel planetary boundary layer; the fluxes of momentum and heat are given by

$$-\overline{w'\mathbf{V}'} = K_m\frac{\partial \mathbf{V}}{\partial z}, \quad (6)$$

$$-\overline{w'T'} = K_h\frac{\partial T}{\partial z}. \quad (7)$$

The flux of momentum in the surface layer (first σ level above the surface) is given by

$$\tau = \rho C_D|\mathbf{V}_S|u_s, \quad (8)$$

where the drag coefficient C_D is set at 0.045 and the subscripts indicate surface layer values. The scheme for computing the eddy diffusivities is from Agee *et al.* (1973). Though of simple form, the variation of K_m with height agrees qualitatively with results ob-

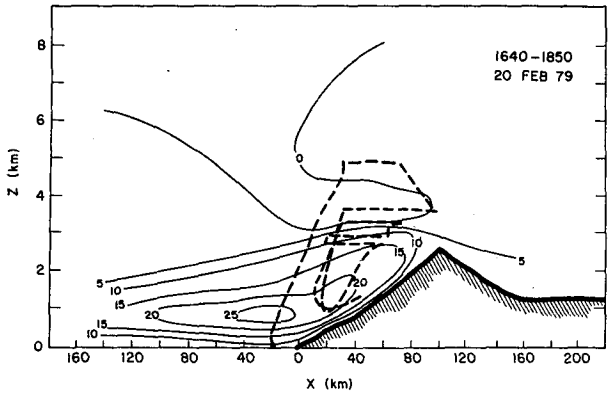

FIG. 5. Mountain-parallel motion components (m s^{-1}) derived from rawinsonde and K/A data for 20 February 1979. Flight track shown by dashed line; flight time listed at top.

tained by using more detailed methods for determining diffusivity values (see Busch *et al.*, 1976). The thickness of the planetary boundary layer is set at 0.2 u^*f^{-1}. Diabatic effects from condensation and melting are not considered here, but will be addressed at a later date.

A total of 40 grid values are used in the horizontal and 15 levels in the vertical. Of the 15 levels, approximately six to eight are within the planetary boundary layer. The staggered horizontal and vertical grid used by Anthes and Warner (1978) is employed. The wind components are specified at the inflow boundaries; the winds at the final outflow grid points are extrapolated from the penultimate grid values. Temperatures are specified on both inflow and outflow boundaries. All boundary values are permitted to change through the boundary-layer mixing processes. In order to help suppress reflection off lateral boundaries, a weighted horizontal diffusion scheme was employed with strongest damping occurring at the boundaries. The porous sponge boundary conditions of Perkey and Kreitzberg (1976), in which tendencies of the prognostic variables are multiplied by weighting factors decreasing from 1.0 in the interior to some small value at the boundary, was also used. These techniques effectively prevented the contaminating boundary effects from reaching the interior of the grid.

b. Case study 20 February 1979

One of the more interesting winter storm days studied during the SCPP 1978–79 field season was the 20 February case. In attempting to characterize the microphysical and dynamical features of the banded precipitation events of the day, the K/A operated within the target area of the American River Basin from 1650–2157 GMT. Rawinsondes were launched at Santa Clara, Sheridan, Fresh Pond and Reno at 1800 GMT. Fig. 5 is a composite cross-section of the mountain-parallel component of the wind based on aircraft measurements and rawinsonde data. The low-level jet is confined below crest level, reaching a maximum speed in excess of 25 m s^{-1} near 1 km. The lateral extent of this barrier wind is over 100 km from the foot of the Sierra Nevada Mountains, stretching across much of the California Valley. Fig. 6 shows the corresponding wind components directed normal to the barrier. Deceleration occurs as the stable air is lifted over the mountains. A significant layer of air is effectively blocked by the barrier, as is evident by the normal wind components directed away from the mountain.

In order to numerically simulate the barrier winds, it was necessary to specify the terrain profile of the Sierra Nevada Range and stability of atmosphere. Terrain heights were specified along a cross section extending from Oakland to Reno using a 20 km grid spacing. An initial temperature profile was constructed using the Sheridan sounding and K/A sounding made on takeoff from McClellan AFB. Specification of initial wind components is problematic. Ideally, the wind profile at locations in the California Valley away from the mountain effects is preferable. It would be possible to investigate the modification of the pressure field along the windward slopes and subsequent adjustment of the wind field, which occurs in the barrier wind development. From the cross section Fig. 6, it is apparent that the large-scale flow was directed primarily normal to the barrier. Below 3 km, the wind speeds were less than approximately 15 m s^{-1}. Although few data exist above the 50 kPa level, the wind appears to increase to over 30 m s^{-1} near 30 kPa. Since barrier wind formation results from the damming up of the low-level flow, proper specification of the wind in the lower part of the atmosphere is most crucial. However, in light of the uncertainty of upper-level wind information, two numerical experiments have been performed. In the first experiment, an initial normal component of 10 m s^{-1} was specified at all levels.

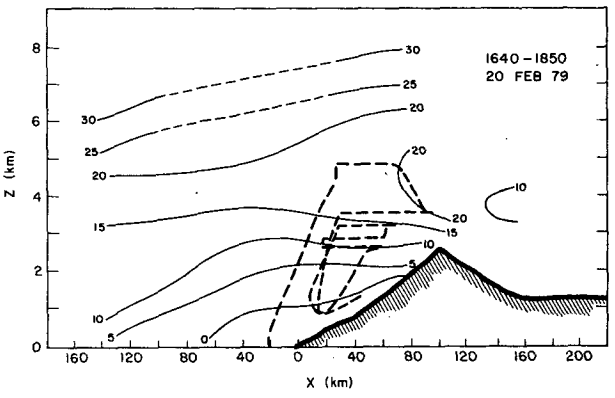

FIG. 6. As in Fig. 5, but for motion components (m s^{-1}) normal to the Sierra Nevada barrier.

The second experiment considers an initial normal component of 10 m s^{-1} below crest level, linearly increasing to 30 m s^{-1} near 30 kPa.

The model equations were integrated for a 10-h period. This corresponds to a non-dimensional time of 3.6 (see Anthes and Warner, 1978); most of the adjustment to a quasi-steady state is complete by this time. Fig. 7 shows the mountain-parallel components after the model integration period. The barrier wind has developed along the terrain slopes and extends into the California Valley. Location of the mountain-parallel jet core compares favorably with the observed winds in Fig. 5. The vertical and horizontal extents match quite well, although the model-calculated winds are somewhat weaker than those observed. The motion components normal to the mountain are shown in Fig. 8. A significant mountain wave is present, tilting upstream with height. Comparison with observation is hampered by the lack of observations on the lee side of the range; the mountain wave is not obvious from the existing information. However, in the low levels along the windward side of the barrier, the model results agree qualitatively with observations summarized in Fig. 6. At upper levels the agreement becomes poor due to the initialization of a 10 m s^{-1} geostrophic normal component at all levels.

Fig. 9 shows the mountain-parallel motion component after the 10-h time integration for the second experiment, in which the initial normal components linearly increase above crest level as suggested by observations. The mountain-parallel winds which have developed do not show the horizontal extent displayed in the first experiment. Also the wind magnitudes have been reduced. However, the qualitative characteristics of the mountain-parallel component agree well with observations. Fig. 10 shows the corresponding normal components of motion after the 10-h integration. The mountain wave is considerably more developed, probably in response to the larger normal wind components above the crest used in the initialization. Again, significant deceleration occurs in the lowest levels along the windward slopes.

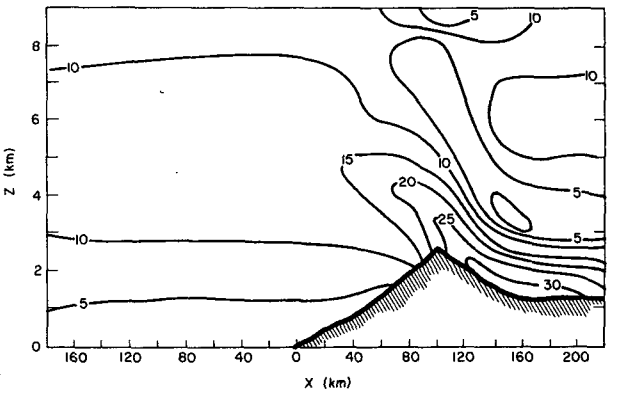

FIG. 8. As in Fig. 7, but for motion component (m s^{-1}) normal to the Sierra Nevada barrier.

In general, the wind patterns from the numerical simulations in Figs. 7–10 are similar to the observed wind features. In agreement with observation, the model mountain-parallel winds are confined below the mountain crest and extend well into the valley. Magnitudes of the calculated mountain-parallel winds after the 10-h time integration period are somewhat less than those observed, but are still very representative. Aside from the model boundary-layer approximations and assumptions, some differences between the numerical experiments and observations may be ascribed to the coarse wind data used in the initialization. A more detailed knowledge of the initial wind components away from the barrier is desirable in order to establish the proper large-scale forcing of the stable air against the mountain. Also, some of the differences may result from the omission of the diabatic heating terms in the thermodynamic equation used in the model. During the forced ascent of air up the barrier, significant latent heat release may occur which may modify the pressure field in the vicinity of the mountain.

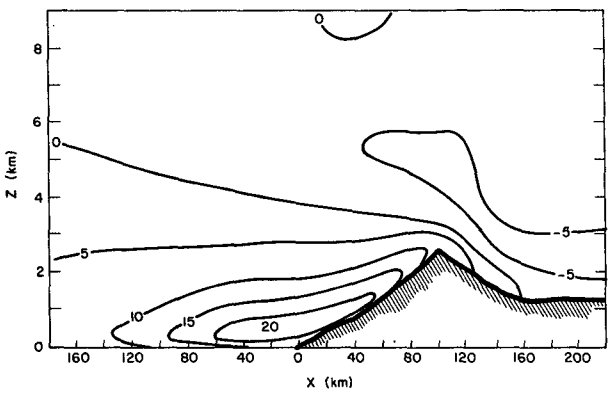

FIG. 7. Mountain-parallel component (m s^{-1}) from Experiment 1 after time integration of 10 hours.

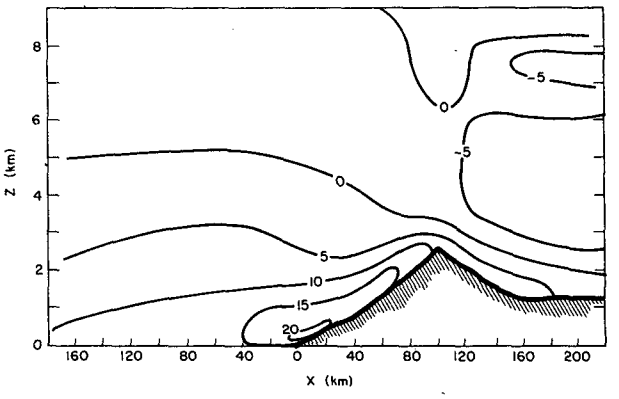

FIG. 9. Mountain-parallel component (m s^{-1}) from Experiment 2 after time integration of 10 h.

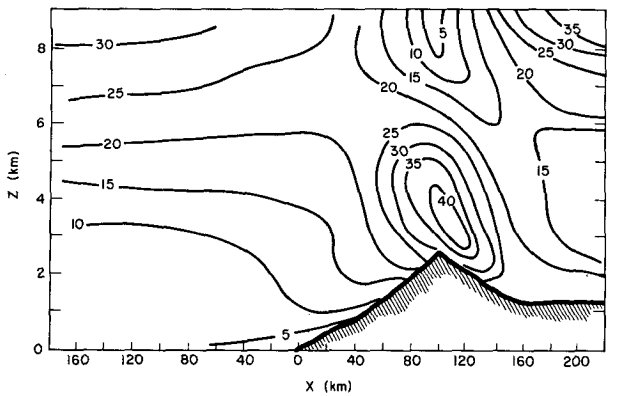

FIG. 10. As in Fig. 9 but for motion component (m s^{-1}) normal to the Sierra Nevada barrier.

5. Summary

Low-level mountain-parallel jets are common along the Sierra Nevada Mountains during winter. The existence of such barrier winds has been firmly established by the data collected using the Wyoming King Air instrumented research aircraft Doppler radar and wind information from the rawinsonde network operated as part of SCPP. Barrier winds have been reported along the Brooks Range in Alaska and in Antarctica, along the Antarctic Peninsula and Transantarctic Mountains. The occurrence of such winds has been attributed to the pressure field created by the damming up of stable air against the barrier due to synoptic-scale forcing. Numerical experiments have been performed with a two-dimensional primitive equation model incorporating terrain representative of the Sierra Nevada range. Using the observed temperature profile at Sheridan, CA and estimates of the wind-field away from the barrier for the 20 February 1979 winter storm case, the model produced a low-level mountain-parallel wind structure in good qualitative agreement with observations.

Acknowledgments. The author expresses his gratitude to J. D. Marwitz for many thoughtful discussions and helpful criticisms. The research was sponsored by the Bureau of Reclamation Service Contract No. 707-83-V0001.

REFERENCES

Agee, E. M., D. E. Brown, T. S. Chen and K. E. Dowell, 1973: A height-dependent model of eddy viscosity in the planetary boundary layer. *J. Appl. Meteor.*, **12,** 409–412.

Anthes, R. A., and T. T. Warner, 1978: The development of hydrodynamic models suitable for air pollution and other mesometeorological studies. *Mon. Wea. Rev.*, **106,** 1045–1078.

Busch, N. E., S. W. Chang and R. A. Anthes, 1976: A multi-level model of the planetary boundary layer suitable for use with mesoscale dynamic models. *J. Appl. Meteor.*, **15,** 909–919.

Godske, C. L., T. Bergeron, J. Bjerknes and R. C. Bundgaard, 1957: *Dynamic Meteorology and Weather Forecasting.* Amer. Meteor. Soc., 800 pp.

Marwitz, J. D., R. E. Stewart, T. S. Karacostas and B. E. Martner, 1978: Cloud Physics in SCPP during 1977–78. Rep. No. AS121, Dept. Atmos. Sci., University of Wyoming, 202 pp.

Nordenskjöld, O., 1911: *Wissenschaftliche Ergebnisse der Schwedischen Suedpolar-Expedition 1901–1903,* Vol. 1. Lithographisches Institut des Generalstabs, Stockholm, Sweden, 232 pp.

Perkey, D. J., and C. W. Kreitzberg, 1976: A time-dependent lateral boundary scheme for limited area primitive equation models. *Mon. Wea. Rev.*, **104,** 744–755.

Schwerdtfeger, W., 1974: Mountain barrier effect on the flow of stable air north of the Brooks Range. *Proc. 24th Alaskan Science Conference,* Geophysical Institute, University of Alaska, Fairbanks, 204–208.

——, 1975: The effect of the Antarctic Peninsula on the temperature regime of the Weddell Sea. *Mon. Wea. Rev.*, **103,** 45–51.

——, 1979: Meteorological aspects of the drift of ice from the Weddell Sea toward the mid-latitude westerlies. *J. Geophys. Res.*, **84,** 6321–6327.

Seaman, N. L., and R. A. Anthes, 1981: A mesoscale semi-implicit numerical model. *Quart. J. Roy. Meteor. Soc.*, **107,** 167–190.

Smith, R. B., 1979: The influence of mountains on the atmosphere. *Advances in Geophysics,* Vol. 21, Academic Press, 87–229.